Medicinal Chemistry Research (2019) 28:1488–1501
https://doi.org/10.1007/s00044-019-02388-4

MEDICINAL CHEMISTRY RESEARCH

ORIGINAL RESEARCH

Novel isoxazole derivatives as potential antiparkinson agents: synthesis, evaluation of monoamine oxidase inhibitory activity and docking studies

Neetu Agrawal[1] · Pradeep Mishra[1]

Received: 9 April 2019 / Accepted: 19 June 2019 / Published online: 1 July 2019

Abstract

Selective monoamine oxidase B inhibitors are potential drug candidates for the treatment of Parkinson's disease. A series of phenyl substituted isoxazole carbohydrazides was designed by structural modification of isocarboxazid, a nonselective MAO inhibitor and evaluated as inhibitors of MAO-A and MAO-B. The compounds were not able to inhibit MAO-A significantly, but most of the compounds exhibited potent inhibitory activity against MAO-B. The enzyme kinetic study of the most active compounds **5d**, 5-phenyl-*N*′-(1-(*p*-tolyl)ethylidene)isoxazole-3-carbohydrazide and **5g**, *N*′-(1-(3,4-dimethoxyphenyl)ethylidene)-5-phenylisoxazole-3-carbohydrazide displayed reversible and competitive MAO-B inhibition. In molecular modeling studies, compounds **5d** and **5g** exhibited strong binding affinity on MAO-B active site. The administration of compounds **5d** and **5g** exhibited prevention of MPTP-induced Parkinsonism as indicated by footprint analysis and horizontal wire tests. Further optimization studies are essential to exploit their potential for MAO-B associated neurodegenerative pathologies.

Keywords Carbohydrazide · Isoxazole · Parkinson's disease · Neurodegenerative diseases · MAO-B inhibitor

Introduction

The monoamine oxidases (MAOs; EC 1.4.3.4) are the flavin adenine dinucleotide (FAD)-dependent enzymes responsible for the metabolism of dietary amines and neurotransmitters as well as oxidation of several xenobiotics. They are preferentially present in the outer mitochondrial membrane of neurons, glia, and many other mammalian cells (Tipton 1986). These enzymes are involved in the oxidative deamination of monoamines, eventually leading to the generation of ammonia, corresponding aldehyde and H_2O_2, that generates toxic hydroxyl radical leading to further aggravation of neurodegeneration (Hauptmann et al. 1996; Jha et al. 2017). The catalytic activities of the MAO enzymes can be blocked by MAO inhibitors, halting the metabolism of monoamine neurotransmitters and thus improving their concentration of in the nerve terminals. This fundamental role of MAOs in neurotransmitter metabolism renders them as potential targets for the exploration of agents to treat psychiatric and neurological disorders.

In mammals, MAO-enzyme exists in two different isoforms in most tissues, i.e., MAO-A and MAO-B. They share 70% similarity (Edmondson et al. 2007) and are differentiated by their amino acid sequences (Bach et al. 1988) tissue distribution (Grimsby et al. 1990), substrate specificities and inhibitor selectivity (Geha et al. 2001). MAO-A preferentially metabolizes bulkier amines like serotonin, adrenaline and noradrenaline and is inhibited by clorgyline selectively. MAO-B preferentially metabolizes smaller amines like β-phenylethylamine and benzylamine and is selectively inhibited by *l*-deprenyl and pargyline (Shih et al. 1999). Some amines like dopamine, tryptamine, and tyramine are the common substrates for both of the isoforms (Weyler et al. 1990; Ma et al. 2004). MAO-A is primarily present in catecholaminergic neurons, while MAO-B is

Supplementary information The online version of this article (https://doi.org/10.1007/s00044-019-02388-4) contains supplementary material, which is available to authorized users.

✉ Neetu Agrawal
kumkumagr.1990@gmail.com

✉ Pradeep Mishra
pmishra51@rediffmail.com

[1] Institute of Pharmaceutical Research, GLA University, Mathura, U.P., India

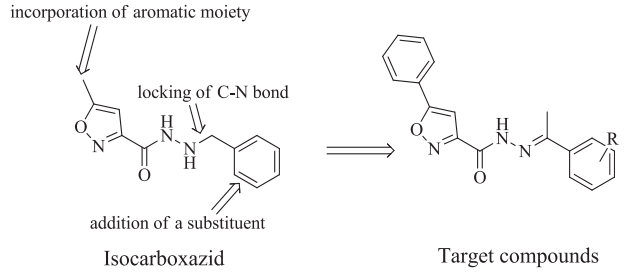

Fig. 1 Design of target compounds

largely present in astrocytes and serotonergic neurons (Bach et al. 1988; Shih et al. 1999).

Due to the difference in substrate specificities, MAO-A and MAO-B are involved in different pathologies; MAO-A inhibitors are used as antidepressants and antianxiety agents while MAO-B inhibitors are used to preclude the progression of Parkinson's disease (PD) and symptoms associated with Alzheimer's disease (AD) (Youdim et al. 2006). However, the nonselective inhibition of MAOs leads to accumulation of tyramine and is associated with serious hypertensive crisis called 'cheese effect' triggered by the consumption of tyramine-rich food. And the irreversible inhibition necessitates de novo biosynthesis of enzymes for the recovery of enzymatic activity (Yamada and Yasuhara 2004). So there is a need for the development of novel selective and reversible MAO inhibitors. Inspired by the findings that on aging the expression of the MAO-B enzyme but not of MAO-A increases in the brain (Nicotra et al. 2004), the chemical compounds are consistently investigated as MAO-B inhibitor for the treatment of neurodegenerative diseases. The compounds with nitrogen and oxygen-containing heterocyclic core are of the great interest for the discovery of such agents (Maccioni et al. 2011; Fabbri et al. 2016; Distinto et al. 2016; Meleddu et al. 2017; Nam et al. 2017).

In the present work, we planned to modify the structure of isocarboxazid (a well known non-selective MAO inhibitor) in an effort to develop newer selective MAO inhibitors from the nonselective one. The heterocyclic nucleus present in isocarboxazid is isoxazole, which is a well-recognized template in heterocyclic chemistry due to the wide variety of activity of its derivatives (Agrawal and Mishra 2018). The other structural feature of isocarboxazid is hydrazide functionality, numerous studies on which have explored its MAO inhibitory potential (Chimenti et al. 2010a, b; Evranos-Aksöz et al. 2014). These findings intrigued the authors to design some new isoxazole derivatives based on isocarboxazid and synthesize them to explore their MAO inhibitory potential. As it is reported that even a small change in the shape of the ligand may be a powerful approach to gain selectivity (Huggins et al. 2012), it was planned to carry out the following modifications on isocarboxazid (i) substitution of methyl group of isocarboxazid with phenyl ring in order to increase the lipophilicity, (ii) introducing double bond between carbon and nitrogen present at hydrazide terminal to lock molecule into a conformation that may be better accommodated by one target than another, (iii) addition of some substituents (such as –Br, $–CH_3$, $–NO_2$) on the phenyl ring present at hydrazide terminal in order to explore the role of substituents present on the phenyl ring in MAO inhibition (Fig. 1).

The synthesized compounds were evaluated for inhibitory activity against MAO-A and MAO-B. The reversibility and kinetic experiments were performed for the two most active compounds to find out the mode of inhibition. Moreover, the compounds showing good in vitro MAO-B inhibitory activity were evaluated for their in vivo anti-parkinsonian potential. The determination of the structure of MAO-B by Binda et al. (2004) and the availability of experimentally determined co-crystals of MAO-B with various inhibitors in the RCSB protein data bank (PDB) have allowed the researchers to carryout computational studies for proposing the preferred binding modes. Thus, molecular docking studies were carried out to gain structural insight into the binding modes of the synthesized compounds in the enzyme active site.

Results and discussion

Chemistry

A series of ten isoxazole carbohydrazides (**5a-j**) was designed and prepared, as shown in Scheme 1. The acetophenone was reacted with diethyl oxalate in the presence of sodium methoxide to give methyl 2,4-dioxo-4-phenylbutanoate (**2**). The compound **2** was then refluxed with hydroxylamine hydrochloride that resulted in cyclization to form methyl 5-phenylisoxazole-3-carboxylate (**3**). The compound **3** was then refluxed in methanol with hydrazine hydrate to give 5-phenylisoxazole-3-carbohydrazide (**4**) (Taha et al. 2015). The treatment of **4** with ten different substituted acetophenones using 3–4 drops of glacial acetic acid resulted in the formation of corresponding hydrazones **5a-j** in very good yields (Taha et al. 2015).

The chemical structures of the synthesized compounds were ascertained with FTIR, ^{1}H NMR, ^{13}C NMR, ESI-MS, and elemental analysis. The IR spectra of the final compounds exhibited a signal at 1698–1669 cm^{-1} belonging to the carbonyl group of the hydrazone. The ^{1}H NMR spectra of the compounds showed the absence of the absorption signal for NH_2 group of hydrazide ($\delta = 4.6$ ppm) of **4**, providing the evidence for the formation of hydrazones.

The literature suggests that the hydrazones exhibit *E*/*Z* geometrical isomerism about C=N bond. However, the

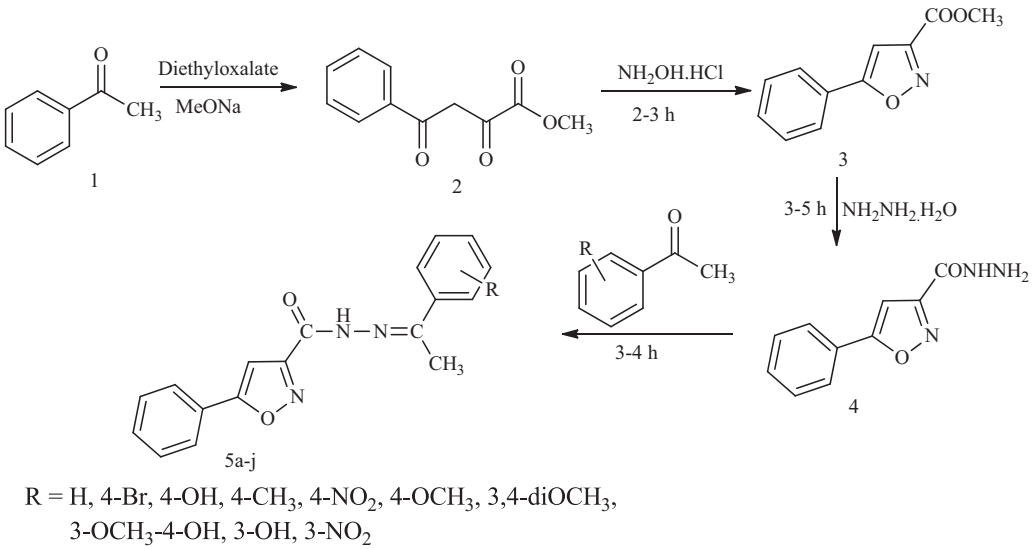

Scheme 1 Synthesis of isoxazole carbohydrazides **5a-j**

analysis of ^{1}H NMR spectra showed that no signal assignable to *Z*-isomer was observed. Generally, the resonance signal for NH proton in hydrazones appears at 14–15 ppm for *Z* and 9–12 ppm for *E*-configuration (Salgın-Gökşen et al. 2013). The NMR spectra of the compounds **5a-j** exhibited a broad singlet between 9.56 and 11.32 ppm, indicating that the preferred configuration in the synthesized compounds is *E*-configuration. In addition, NOESY cross-peaks were studied for compound **5e** which had NH proton signal at highest value of δ 11.32 ppm to further confirm the configuration of synthesized hydrazones. The proton at δ 11.32 ppm displayed NOESY cross-peak with the methyl protons, which confirmed the *E*-isomer. The mass spectra of the compounds displayed the characteristic peaks. The elemental analyses results were within ±0.4% of the calculated values.

In vitro MAO-inhibition

The in vitro MAO-inhibitory activity and selectivity of new isoxazole carbohydrazides (**5a-j**) and reference compounds were determined using crude rat brain mitochondrial suspension by a fluorimetric assay method (Chimenti et al. 2007). Clorgyline and pargyline were used as reference inhibitors for MAO-A and MAO-B, respectively. The results are expressed in terms of percentage inhibition and IC_{50} values (Table 1). The IC_{50} values were determined only for the compounds showing more than 50% inhibition at 50 µM (the highest concentration tested). It can be seen that all the compounds showed non-significant activity against MAO-A at 50 µM while most of the compounds inhibited MAO-B significantly in the micromolar to the nanomolar range indicating the high selectivity of compounds for MAO-B. Overall, our efforts in the tailoring of the isocarboxazid molecule to impart selectivity for one isoform of MAO were quite successful. The compounds **5a**, **5b**, **5d**, **5f** and **5g** displayed about 95% inhibition; compound **5j** displayed 88% inhibition while rest of the compounds exhibited less than 50% inhibition of MAO-B activity at 50 µM. It is suggested that substituents like halogen, methyl, methoxy (**5b**, **5d**, **5f**, **5g**) at 4-position might have strengthened the MAO-B inhibitory activity. Compound **5d** with a methyl group at the *para* position of phenyl ring appeared as a most potent MAO-B inhibitor (IC_{50} value of 0.0051 ± 0.0009 µM), followed by compound **5g** with methoxy substituent at the 3- and 4-positions of phenyl ring (IC_{50} = 0.0059 ± 0.0007 µM).

The replacement of these groups with hydrogen (**5a**) and electron withdrawing bromo substituent led to compound **5b** with less but appreciable MAO-B inhibitory activity. However, substitutions of phenyl ring with hydroxy at 3 or 4-positions (**5c, 5h**, **5i**) dramatically decreased the MAO-B inhibitory activity. Interestingly, the introduction of a nitro substituent at 4-position (**5e**) diminished the MAO-B inhibitory activity whereas at 3-position led to compound **5j** with significant retention of the MAO-B inhibitory activity. Thus, it was observed that the introduction of the lipophilic moieties such as bromo, methyl and methoxy on the hydrophobic aryl ring at the hydrazide terminal increased the MAO-B inhibitory activity, whereas the presence of hydrophilic motifs like hydroxy and nitro groups caused a decrease in the MAO-B inhibitory activity. The results provide insight into the important role of the nature of the substitution on phenyl group present at hydrazide terminal for the development of potent MAO-B inhibitors.

Table 1 IC_{50} values and percentage inhibition for inhibitory effects of **5a-j** on MAO-A and MAO-B

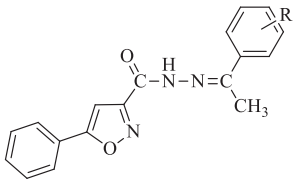

Compound	R	MAO-A (% inhibition)[a]	MAO-B (% inhibition)[a]	MAO-B (IC_{50}; μM)[b]
5a	-H	*	94.85	0.0634 ± 0.0026
5b	4-Br	*	95.91	0.0663 ± 0.0019
5c	4-OH	*	28.56	nd
5d	4-CH_3	*	95.21	0.0051 ± 0.0009
5e	4-NO_2	7.85	43.12	nd
5f	4-OCH_3	*	95.64	0.0752 ± 0.0022
5g	3,4-diOCH_3	*	95.85	0.0059 ± 0.0007
5h	3-OCH_3,4-OH	27.85	18.90	nd
5i	3-OH	*	35.90	nd
5j	3-NO_2	12.47	88.04	0.710 ± 0.018
Clorgyline	–	89.09 (0.0011 ± 0.00084)[c]	–	–
Pargyline	–	–	94.14	0.0234 ± 0.0021

[a]% inhibition at 50 μM (highest tested concentration)

[b]Each IC_{50} value is the mean ± S.E.M. ($n = 3$)

[c]IC_{50} value in μM

nd not determined

*Inactive at 50 μM (higher concentration of compounds led to precipitation)

Reversibility studies

Another aim of the present study was to determine whether the compounds **5d** and **5g** are reversible or irreversible enzyme inhibitor. As reversible MAO-B inhibitors pose fewer side effects than irreversible ones, these are considered more promising (Kumar et al. 2016). A dilution method was used with pargyline (irreversible inhibitor) as the standard (Copeland 2005). Both the compounds **5d** and **5g** were found to be reversible as evidenced by the recovery of MAO-B activity after dilution with the substrate (Table 2).

Table 2 Reversibility studies of MAO-B inhibition by derivatives **5d**, **5g** and reference inhibitor

Compound	Slope (AUF/t) [%][a]
5d	72.90 ± 4.8
5g	92.77 ± 0.32
Pargyline	10.59 ± 0.19

[a]Percentage values represent the mean ± S.E.M. of three experiments ($n = 3$) relative to control. ~91% indicates reversibility, whereas ~9% indicates irreversible inhibition

Enzyme kinetic studies

The kinetic analysis was carried out for these two MAO-B inhibitors **5d** and **5g** to have an understanding of the mode of MAO inhibition. Sets of Lineweaver-Burk plots were plotted in the absence and presence of different concentrations (½ × IC_{50}, 1 × IC_{50} and 1½ × IC_{50}) of compounds **5d** and **5g**. The set consisted of four graphs, each plotted by estimating the MAO-B catalytic rate at various substrate concentrations (250–1000 μM). The observations that the

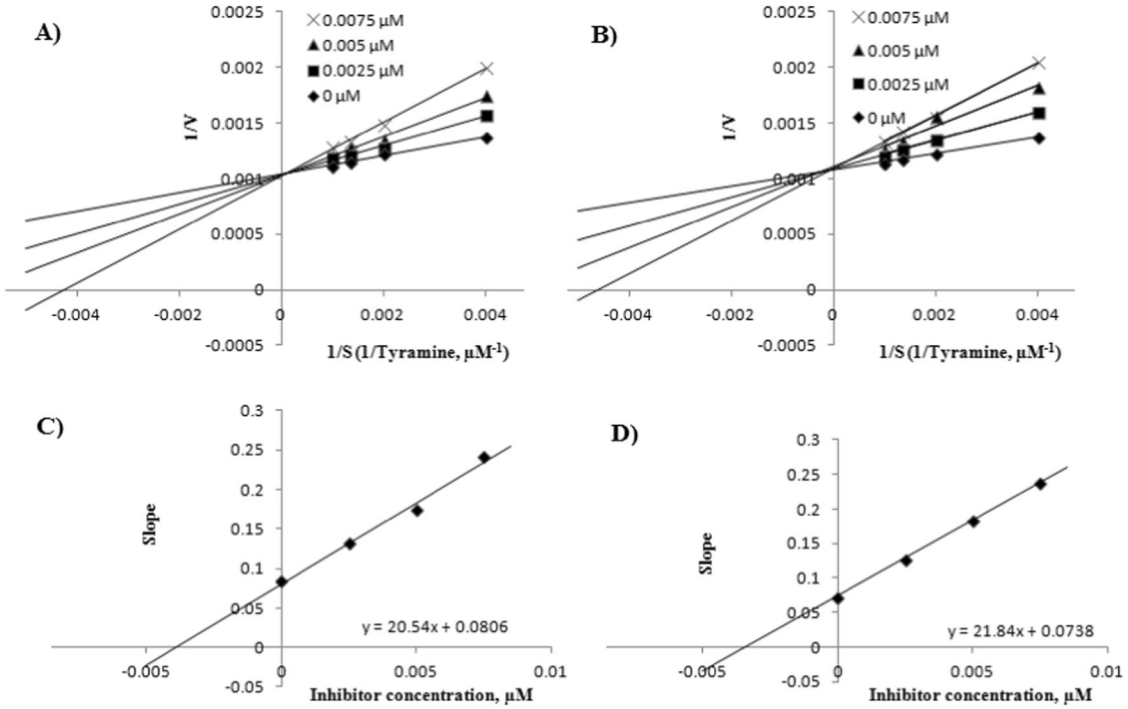

Fig. 2 Lineweaver-Burk plots of rat brain MAO-B-activity in the absence (control) and presence of different concentrations of compound **5d** (**a**) and compound **5g** (**b**). Replots of the slopes of the Lineweaver-Burk plots versus inhibitor **5d** concentration (**c**) inhibitor **5g** concentration (**d**)

lines were linear and intersected on the *y*-axis (Fig. 2) suggest that **5d** and **5g** are the competitive inhibitors of MAO-B. The replots of the slopes of the Lineweaver-Burk plots *versus* inhibitor concentration are shown in Fig. 2, and the *Ki* was calculated as −0.0039 µM for **5d** and −0.0034 µM for **5g**.

Molecular docking studies

The docking studies for all the compounds synthesized were carried out to confirm the binding and orientations of ligands against human MAO-B (PDB ID: 2V60). There are two hydrophobic cavities in the active site of the enzyme, the entrance cavity (~300 $Å^3$) and the substrate cavity (~400 $Å^3$) which are separated by Phe168, Leu171, Ile199 and Tyr326 side chains (Kumar et al. 2016). The two nearly parallel tyrosyl residues (Tyr398 and Tyr 435) and FAD form an aromatic cage (Edmondson et al. 2007).

The docking was performed using Autodock 4.2, and the validation of docking was performed by the super-imposition of the co-crystallized ligand to the docked ligand with RMSD less than 2 Å. Interestingly, all of the compounds showed the same orientation, i.e., the phenyl ring at imino terminal oriented towards the entrance cavity while the aryl substituted isoxazole part oriented towards the substrate cavity. Further investigation of the ligand-protein complexes showed that the compounds were occupied at the wide active site cavity formed by the amino acid residues Gln206, Tyr326, Cys172, Ile316, Leu171 and Ile199. This proves that the synthesized compounds possess significant binding interaction at the active site of the MAO-B enzyme. In addition, most of the inhibitors were stabilized by hydrogen bonds, hydrophobic and π-π interactions in the pocket of the enzyme.

We focused our attention on the binding interactions of the most active compounds **5d** and **5g** (Fig. 3). The docking score of **5d** was found to be −7.93 Kcal/mol and its interaction revealed that the isoxazole and unsubstituted phenyl rings displayed a π-π interaction with Tyr435 and Phe343 respectively. Further, a π-π interaction was also observed between Tyr326 and methyl substituted phenyl ring. The amino nitrogen atom of the hydrazone linker was stabilized by H-bond interactions with the oxygen atom of Ile198. Likewise, the oxygen atom of the isoxazole was hydrogen bonded to the OH group of Tyr435. Moreover, the methyl group present on phenyl ring was involved in π-alkyl interactions with Leu167, Ile316 and Tyr326 that may explain the observation that methyl substitution on the phenyl side chain of **5d** enhances MAO-B inhibitory potency. It also showed important hydrophobic interaction with Tyr60, Gln206, Leu328, and Met341 residues.

Similarly, the binding pose of **5g** (docking score −6.88 Kcal/mol) at the MAO-B binding site revealed that the dimethoxy phenyl group extends toward the entrance cavity

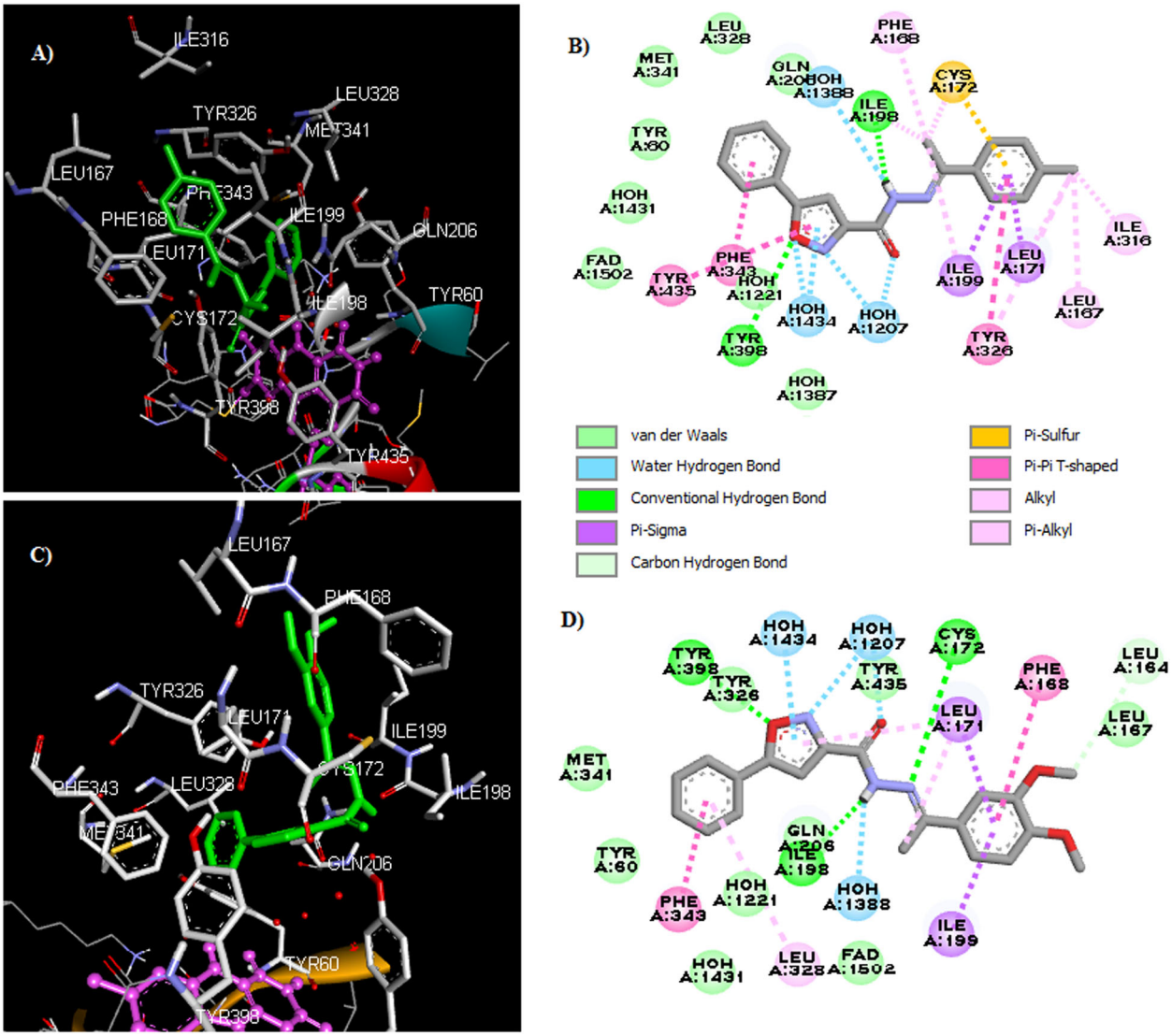

Fig. 3 **a** Binding mode of **5d** (green) in the MAO-B binding pocket. **b** Binding interactions of **5d** with the active site of MAO-B. **c** Binding mode of **5g** (green) in the MAO-B binding pocket. **d** Binding interactions of **5g** with the active site of MAO-B. The cofactor FAD is displayed as purple ball and stick. Selected residues are labeled and displayed as sticks

leaving the Ile199 in the open-gate conformation and is lined by residues Leu164, Leu167, Phe168, Leu171, Ile198, and Ile199. The dimethoxy bearing phenyl group is sandwiched between Phe168 and Ile199 forming π-π and π-σ interactions respectively. In addition, the unsubstituted phenyl ring was involved in π-π interaction with Phe343. Moreover, three hydrogen bond interactions were also observed between isoxazole oxygen and hydroxy group of Tyr398; amido and the carbonyl oxygen of Ile198; and imine and sulfhydryl group of Cys172. The methoxy group at 3-position showed interaction with Leu164. It also showed the crucial hydrophobic interaction with residue Tyr60, Cys172, Gln206, Met341, Tyr326, Leu328, Tyr398, Tyr435, Leu164, and Leu167.

Prediction of ADME properties

Poor pharmacokinetic properties are one of the major reasons for the failure of the development of drug candidates in the early stages. Thus in the present study, in silico ADME properties and drug-likeness for the synthesized compounds **5a-j** were predicted using MedChem Designer 3.0 (http://www.simulations-plus.com). The values of predicted parameters are present in Table 3. According to these data, all designed compounds (**5a-j**) except **5b** (MlogP > 4.15) follow the Lipinski's rule (Lipinski et al. 2012) without causing any violation.

Ideally, the value of logP should not be greater than 5 for tissue absorption and for brain penetration it should not be

Table 3 In silico ADME evaluation of title compounds **5a-j**

Compound	MlogP[a]	S + logP[b]	S + logD[c]	MWt[d]	MNO[e]	TPSA[f]	HBDH[g]	Rule of 5[h]
5a	3.715	3.833	3.832	305.338	5	67.49	1	0
5b	4.329	4.572	4.571	384.239	5	67.49	1	1
5c	3.211	3.961	3.948	321.338	6	87.72	2	0
5d	3.947	4.152	4.151	319.365	5	67.49	1	0
5e	3.801	4.254	4.253	350.336	8	113.31	1	0
5f	3.443	4.055	4.054	335.365	6	76.72	1	0
5g	2.911	3.956	3.956	365.391	7	85.95	1	0
5h	2.684	3.767	3.737	351.364	7	96.95	2	0
5i	3.211	3.946	3.941	321.338	6	87.72	2	0
5j	3.801	3.938	3.937	350.336	8	113.31	1	0

[a]predicted logP using Moriguchi's model

[b]predicted log of the octanol/water partition coefficient using the Simulation Plus ANNE model

[c]predicted logD at pH 7.4 using the Simulation Plus ANNE model

[d]Molecular weight

[e]the number of hydrogen bond acceptors (total number of nitrogen and oxygen atoms)

[f]topological polar surface area

[g]number of hydrogen bond donor protons

[h]number of Lipinski's rule of 5 violations

more than 4.0 (Waterhouse 2003). From the data presented in Table 3, it can be seen that all compounds except **5b** fulfill these requirements and thus can be predicted to have good oral bioavailability and brain penetration ability.

Acute toxicity

The compound **5d** and **5g** were then evaluated for their acute oral toxicity in mice according to OECD425 guidelines (OECD 2008). The test compounds demonstrated good safety margins, and the LD_{50} dose was found to be 2000 mg Kg^{-1}.

Neurotoxicity screening

Compounds **5d** and **5g** were evaluated for neurotoxicity using a rotarod apparatus. The animals fed with **5d** and **5g** (200 mg Kg^{-1}) were able to stay on accelerating rotarod for more than 60 s leading to the conclusion that both the compounds were non-neurotoxic.

Motor Behavioral test

To verify the in vivo efficiency of the compounds **5d** and **5g** as a MAO-B inhibitor, experiments were conducted on the MPTP (1-methyl-4-phenyl-1,2,3,6-tetrahydropyridine)-induced Parkinson's animal model (Jackson-Lewis and Przedborski 2007). The mice were treated with standard drug Safinamide (30 mg Kg^{-1}, *p.o.*) or compounds **5d** and **5g** at three dose levels of 50, 100 and 200 mg Kg^{-1}, *p.o.* for three consecutive days (day 0, 1 and 2). After the drug

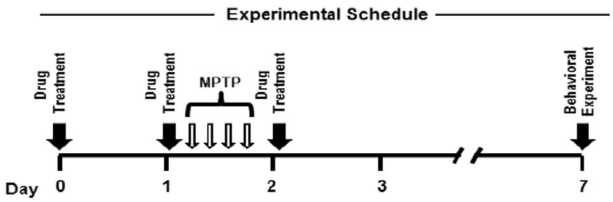

Fig. 4 The experimental schedule for in vivo antiparkinsonian activity

administration on day 1, mice were administered MPTP (20 mg Kg^{-1}, *i.p.*) four times at 2 h intervals. The behavioral evaluation of experimental animals was done on day 7 to assess the motor ability (Fig. 4).

PD patients may exhibit rigidity and abnormal gait with trouble in walking and balancing and reduced stride length. In the footprint test, the base width and stride length of both fore and hind-paws were measured which are useful to evaluate motor functions in mice treated with neurotoxins such as MPTP (Geed et al. 2014). Figure 5 shows the effect of **5d** and **5g** treatment on base width differences and mean stride length in MPTP-treated mice. No significant differences among the groups were observed in the fore- and hind-paw base width ($p > 0.05$) as revealed by one-way ANOVA. However, a significant decrease in stride length for both fore- and hind-paw ($p < 0.05$) was observed in mice treated with MPTP, which were significantly improved by the treatment of **5d** and **5g**. Post-hoc analysis revealed that there was no significant difference between the 100 and 200 mg/Kg doses of the compounds **5d** and **5g**. Thus, the inhibitors **5d** and **5g** (100 mg/Kg) were able to improve the abnormal posture and gait of mice induced by MPTP.

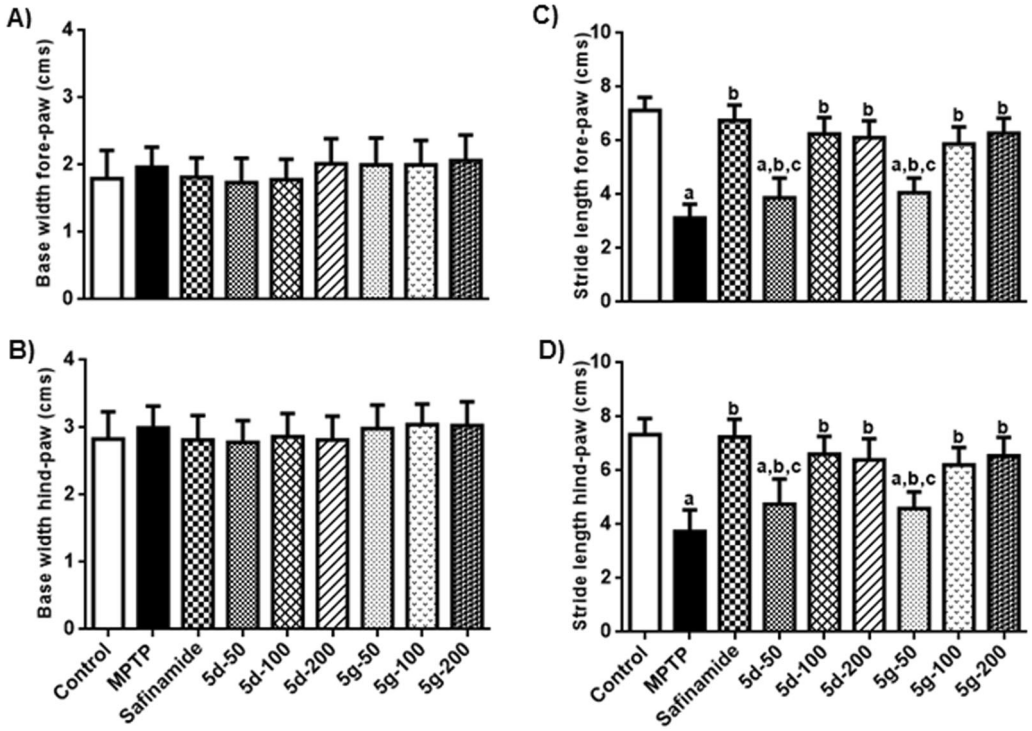

Fig. 5 **a** Fore-paw base width, **b** hind-paw base width, **c** fore-paw stride length, and **d** hind-paw stride length in the footprint test. All values are mean ± SD. $^{a}p < 0.05$ compared to control, $^{b}p < 0.05$ compared to MPTP group, and $^{c}p < 0.05$ compared to Safinamide group [one-way ANOVA followed by Student-Newman-Keuls test]

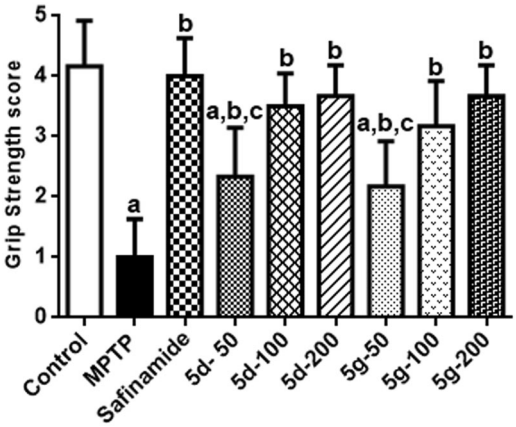

Fig. 6 Grip strength score in the horizontal wire test. All values are mean ± SD. $^{a}p < 0.05$ compared to control, $^{b}p < 0.05$ compared to MPTP group, and $^{c}p < 0.05$ compared to Safinamide group [one-way ANOVA followed by Student-Newman-Keuls test]

Further, the horizontal wire test was performed to estimate the muscle relaxation and motor coordination in experimental animals. As shown in Fig. 6, MPTP decreased the grip strength score in model mice. The decrease in the grip strength was significantly improved in the experimental animals treated with **5d** and **5g**, indicated by the improved grip strength score in those animals. Thus, the inhibitors **5d** and **5g** were able to improve the muscle strength of mice that was impaired by MPTP. The results were parallel to what was observed with the reference drug, safinamide. Collectively, the motor behavioral study revealed that **5d** and **5g** have the potential to improve MPTP-induced impairment in motor functions in terms of improving gait behavior and grip strength.

Conclusion

A new series of *N*'-(1-(substituted phenyl)ethylidene)-5-phenylisoxazole-3-carbohydrazide derivatives (**5a-j**) was prepared and screened for in vitro MAO inhibitory activity. Our strategy to design selective compounds from non-selective MAO inhibitor isocarboxazid was successful as most of the compounds were selective towards MAO-B. The enzyme kinetic studies revealed that the inhibitors **5d** and **5g** were reversible and competitive. The docking studies further unlocked the binding site interactions of the potent inhibitors, and it was found that compounds fit well in the active site of MAO-B near the FAD cofactor. The synthesized compounds were subjected to in silico ADME evaluation. All the compounds displayed favorable ADME profile and thus predicted to have good oral bioavailability. Compounds **5d** and **5g** were able to significantly prevent MPTP-induced neurodegeneration as revealed by motor behavioral assessment using the footprint and horizontal

wire tests. Consequently, we have fulfilled our initial expectations, that highly selective MAO-B inhibitors have been discovered having the capability to prevent MPTP-induced neurodegeneration. Thus the active compounds **5d** and **5g** obtained in this series can be promising leads for the development of isoxazole-based potent MAO-B inhibitors for the treatment of PD.

Experimental section

Materials and methods

All the chemicals, reagents and drugs were procured from Sigma-Aldrich and Merck, and used as such. The completion of the reactions and the purity of compounds at each step were verified using thin layer chromatography (TLC). The adsorbent used was silica gel G and the detecting agent used was iodine vapor. Melting points were determined by open capillary melting point apparatus and presented without correction. IR spectra (in KBr) were recorded on a Shimadzu IR Affinity-1 FTIR spectrophotometer, using DRS 8000A accessory technique. ^{1}H NMR and ^{13}C NMR spectra were recorded in DMSO-d6 or $CDCl_3$ at ambient temperature on a Bruker Avance II spectrometer at 400 MHz (100 MHz for ^{13}C) at Panjab University, Chandigarh (India). Chemical shifts (δ) are expressed in parts per million (ppm) using TMS as an internal standard. Coupling constants J are expressed in Hertz (Hz). Spin multiplicities are reported as s (singlet), d (doublet), dd (doublet of doublets), t (triplet), q (quartet) or m (multiplet). Mass spectra were recorded on Waters, Q-TOF Micromass (ESI) at Sophisticated Analytical Instrumentation Facility (SAIF), Panjab University, Chandigarh (India). Elemental analyses for C, H and N were determined with EuroVector E 3000 Elemental Analyzer at SAIF, CDRI, Lucknow (India).

Chemistry

Synthesis of methyl 2,4-dioxo-4-phenylbutanoate (2)

For the synthesis of compound **2**, the procedure of Veeraswamy et al. (2012) was followed with some modifications. Sliced sodium metal (1.15 g) was added to methanol (25 mL) maintained at 0–10 °C in an ice bath and was kept stirring. Acetophenone (6.0 mL, 0.05 mol) was added slowly and then the diethyl oxalate (8.0 mL, 0.06 mol) was added drop-wise and stirred for an hour while maintaining the temperature as stated above till the product separated. The solid was dissolved in distilled water and then extracted with diethyl ether to remove unreacted acetophenone, if any. Then dilute acetic acid was added to precipitate out the product which was separated and the recrystallization was done using ethanol to give compound **2** (6.69 g; 65.0%; m.p.: 60–61 °C, *lit*. 61 °C) (Veeraswamy et al. 2012).

Synthesis of methyl 5-phenylisoxazole-3-carboxylate (3)

Compound **2** (4.12 g, 0.02 mol) and hydroxylamine hydrochloride (1.67 g, 0.024 mol) were and refluxed for 2–3 h in methanol (200 mL), while judging the completion of the reaction by TLC (hexane:ethyl acetate 3:1). Methanol was removed under vacuum and the content was poured over crushed ice. The solid separated out was filtered, washed with water and recrystallized from ethanol to obtain compound **3** (3.66 g; 90.1%; m.p.: 86–87 °C, *lit*. 86–88 °C) (Veeraswamy et al. 2012).

Synthesis of 5-phenylisoxazole-3-carbohydrazide (4)

The compound **3** (2.1 g, 0.010 mol) was dissolved in 50 mL of methanol, and then hydrazine hydrate (0.5 mL, 0.0015 mol) was added. The reaction mixture was refluxed for 3–5 h. The completion of the reaction was judged by running TLC (hexane:ethyl acetate 3:1). The contents were cooled and poured on crushed ice. A fluffy white precipitate obtained was filtered, washed with water and dried to give **4** (1.81 g; 86.0%; m.p.: 148–149 °C, *lit*. 148–153 °C) (Taha et al. 2015).

General Procedure for the synthesis of final products (5a-j)

The carbohydrazide **4** (1.0 g, 0.005 mol) was dissolved in methanol (100 mL) and the desired acetophenone (0.005 mol) was added. Then 4–5 drops of glacial acetic acid were added and the contents were refluxed for 3–4 h. The product which got separated was filtered after cooling, washed with ether to remove unreacted acetophenone, if any and dried to get the final products **5a-j** (Taha et al. 2015). R_f values for **5a-j** were determined using $CHCl_3$/methanol/toluene in 7:1:2 as a solvent system.

5-phenyl-*N*′-(1-phenylethylidene)isoxazole-3-carbohydrazide (5a)

Buff colored needle-shaped crystalline (94.4%); $R_f = 0.75$; m.p.: 189–190 °C; ^{1}H NMR (300 MHz, $CDCl_3$): $\delta = 2.41$ (s, 3H, CH_3), 7.11 (s, 1H, isoxazole CH), 7.40–7.42 (m, 3H, Ar-H), 7.49–7.52 (m, 3H, Ar-H), 7.80–7.82 (m, 2H, Ar-H), 7.86–7.89 (m, 2H, Ar-H), 9.71 (s, 1H, CONH); ^{13}C NMR (75 MHz, $CDCl_3$): 19.66 (CH_3), 99.87 (isoxazole CH), 126.15 (2C), 126.56, 126.86 (2C), 128.49 (2C), 129.24 (2C), 130.06, 130.95, 137.41, 154.05, 154.93, 158.98, 171.92; IR (KBr): $\tilde{\nu} = 3312.88$ (NH), 3047.66 (Ar C-H), 1680.07 (NH-C=O), 1572.05 (C=N), 1518.04 (C=C, isoxazole), 1449.57 cm^{-1} (Ar C=C); ESI-MS (*m/z*): 306.19

(M + 1); Anal. for $C_{18}H_{15}N_3O_2$: calcd: C 70.81, H 4.95, N 13.76, found: C 70.94, H 5.18, N 13.48.

N′-(1-(4-bromophenyl)ethylidene)-5-phenylisoxazole-3-carbohydrazide (5b)

White shiny needle-shaped crystalline (48.0%); $R_f = 0.68$; m.p.: 214–215 °C; ^{1}H NMR (400 MHz, $CDCl_3$): $\delta = 2.39$ (s, 3H, CH_3), 7.42 (s, 1H, isoxazole CH), 7.54–7.61 (m, 5H, Ar-H), 7.80–7.82 (m, 2H, Ar-H), 7.93–7.95 (m, 2H, Ar-H), 11.03 (s, 1H, CONH). ^{13}C NMR (100 MHz, $CDCl_3$):: $\delta =$ 14.37 (CH_3), 99.99 (isoxazole CH), 123.42, 125.68 (2C), 126.23, 128.42 (2C), 129.10 (2C), 130.65, 131.19, 136.71 (2C), 155.50, 155.79, 158.77, 170.41; IR (KBr): $\tilde{\nu} =$ 3287.81 (NH), 3055.38 (Ar C-H), 1680.07 (NH-C=O), 1546.01 (C=N), 1485.25 (C=C, isoxazole), 1444.75 cm^{-1} (Ar C=C); ESI-MS (*m/z*): 385.30 (M + 1), 386.28 (M + 2); Anal. for $C_{18}H_{14}BrN_3O_2$: calcd: C 56.27, H 3.67, N 10.94, found: C 56.49, H 3.75, N 10.68.

N′-(1-(4-hydroxyphenyl)ethylidene)-5-phenylisoxazole-3-carbohydrazide (5c)

Buff colored crystalline (85.7%); $R_f = 0.52$; m.p.: 235–236 °C; ^{1}H NMR (300 MHz. DMSO-d6): $\delta = 2.31$ (s, 3H, CH_3), 6.82–6.84 (m, 2H, Ar-H), 7.49–7.58 (m, 5H, 4 Ar-H, isoxazole CH), 7.73–7.75 (m, 2H, Ar-H), 7.96–7.98 (m, 1H, Ar-H), 9.90 (s, 1H, CONH), 10.99 (s, 1H, OH); ^{13}C NMR (75 MHz. DMSO-d6): $\delta = 14.92$ (CH_3), 100.68 (isoxazole CH), 115.62 (2C), 126.28 (2C), 126.73, 128.18, 128.80 (2C), 129.86 (2C), 131.40, 155.74, 158.61, 159.64, 159.76, 170.76; IR (KBr): 3342.78 (OH), 3297.45 (NH), 3071.77 (Ar C-H), 1676.21 (NH-C=O), 1540.23 (C=N), 1514.19 (C=C, isoxazole), 1448.60 cm^{-1} (Ar C=C); ESI-MS (*m/z*): 322.40 (M + 1); Anal. for $C_{18}H_{15}N_3O_3$: calcd: C 67.28, H 4.71, N 13.08, found: C 67.45, H 5.04, N 12.71.

5-phenyl-*N′*-(1-(*p*-tolyl)ethylidene)isoxazole-3-carbohydrazide (5d)

White shine crystalline (77.6%); $R_f = 0.80$; m.p.: 197–198 °C; ^{1}H NMR (300 MHz, $CDCl_3$): $\delta = 2.37$–2.42 (m, 6H, 2 CH_3), 7.10 (s, 1H, isoxazole CH), 7.20–7.22 (m, 1H, Ar-H), 7.35–7.50 (m, 4H, Ar-H), 7.73–7.79 (m, 4H, Ar-H), 9.67 (s, 1H, CONH). ^{13}C NMR (75 MHz, $CDCl_3$): $\delta = 13.33$ (CH_3), 21.34 (Ar-CH_3) 99.51 (isoxazole CH), 125.96 (2C), 126.39, 126.58, 126.77 (2C), 129.19 (2C), 130.44, 130.88, 134.56, 140.27, 154.11, 154.83, 158.63, 171.85; IR (KBr): 3364.96 (NH), 3065.02 (Ar C-H), 1698.40 (NH-C=O), 1570.12 (C=N), 1511.29 (C=C, isoxazole), 1446.67 cm^{-1} (Ar C=C); ESI-MS (*m/z*): 320.42 (M + 1), Anal. for $C_{19}H_{17}N_3O_2$: calcd: C 71.46, H 5.37, N 13.16, found: C 71.88, H 5.64, N 12.88.

N′-(1-(4-nitrophenyl)ethylidene)-5-phenylisoxazole-3-carbohydrazide (5e)

Pale yellow crystalline (56.5%); $R_f = 0.54$; m.p.: 247–248 °C; ^{1}H NMR (300 MHz, DMSO-d6): $\delta = 2.50$ (s, 3H, CH_3), 7.38–7.59 (m, 4H, 3Ar-H, isoxazole CH), 7.97–7.98 (m, 2H, Ar-H), 8.12–8.19 (m, 2H, Ar-H), 8.30–8.32 (m, 2H, Ar-H), 11.30 (s, 1H, CONH); ^{13}C NMR (75 MHz, DMSO-d6): $\delta =$ 18.88 (CH_3), 101.76 (isoxazole CH), 123.26 (2C), 126.15 (2C), 127.67 (2C), 128.09, 128.69 (2C), 130.34, 141.08, 148.52, 149.18, 160.54, 162.39, 170.81; IR (KBr): 3345.67 (NH), 3077.56 (Ar C-H), 1698.40 (NH-C=O), 1558.55 (C=N), 1516.11 (C=C, isoxazole), 1492.00 (Ar N-O), 1448.60 (Ar C=C), 1346.37 cm^{-1} (Ar N-O); ESI-MS (*m/z*): 351.53 (M + 1); Anal. for $C_{18}H_{14}N_4O_4$: calcd: C 61.71, H 4.03, N 15.99, found: C 62.01, H 4.34, N 16.24.

N′-(1-(4-methoxyphenyl)ethylidene)-5-phenylisoxazole-3-carbohydrazide (5f)

White shiny needle-shaped crystalline (81.8%); $R_f = 0.64$; m.p.: 201–203 °C; ^{1}H NMR (300 MHz, $CDCl_3$): $\delta = 2.29$ (s, 3H, CH_3), 3.76 (s, 3H, OCH_3), 6.83–6.85 (m, 2H, Ar-H), 7.02 (s, 1H, isoxazole CH), 7.38–7.43 (m, 3H, Ar-H), 7.77–7.78 (m, 4H, Ar-H), 9.56 (s, 1H, CONH). ^{13}C NMR (75 MHz, $CDCl_3$): $\delta = 13.26$ (CH_3), 55.36 (OCH_3) 99.52 (isoxazole CH), 113.80 (2C), 125.97 (2C), 126.61, 128.39 (2C), 129.19 (2C), 129.89, 130.89, 153.86, 154.79, 158.68, 161.22, 171.84; IR (KBr): 3360.14 (NH), 3000.40 (Ar C-H), 1695.50 (NH-C=O), 1539.26 (C=N), 1507.43 (C=C, isoxazole), 1446.67 cm^{-1} (Ar C=C). ESI-MS (*m/z*): 336.42 (M + 1); Anal. for $C_{19}H_{17}N_3O_3$: calcd: C 68.05, H 5.11, N 12.53, found: C 68.37, H 5.43, N 12.78.

N′-(1-(3,4-dimethoxyphenyl)ethylidene)-5-phenylisoxazole-3-carbohydrazide (5g)

White shiny needle-shaped crystalline (64.6%): $R_f = 0.68$; m.p.: 168–169 °C; ^{1}H NMR (300 MHz, $CDCl_3$): $\delta = 2.38$ (s, 3H, CH_3), 3.91 (s, 3H, OCH_3), 3.97 (s, 3H, OCH_3), 6.86 (d, 1H, Ar-H, $J = 5.1$ Hz), 7.27 (s, 1H, isoxazole CH), 7.33 (dd, 1H, Ar-H, $J = 1.2$ Hz, 1.2 Hz), 7.46–7.50 (m, 3H, Ar-H), 7.60 (d, 1H, Ar-H, $J = 1.2$ Hz) 7.80–7.82 (m, 2H, Ar-H), 9.66 (s, 1H, CONH). ^{13}C NMR (75 MHz, $CDCl_3$): $\delta = 13.31$ (CH_3), 55.99 (OCH_3), 56.06 (OCH_3), 99.46 (isoxazole CH), 109.31, 110.32, 120.25, 125.98 (2C), 126.58, 129.19 (2C), 130.20, 130.91, 148.99, 150.99, 153.97, 154.78, 158.64, 171.88; IR (KBr): 3319.63 (NH), 2999.44 (Ar C-H), 1684.89 (NH-C=O), 1595.51 (C=N), 1517.08 (C=C, isoxazole), 1442.82 cm^{-1} (Ar C=C); ESI-MS (*m/z*): 366.28 (M + 1); Anal. for $C_{20}H_{19}N_3O_4$: calcd: C 65.74, H 5.24, N 11.50, found: C 65.93, H 5.58, N 11.18.

N′-(1-(3-hydroxy-4-methoxyphenyl)ethylidene)-5-phenylisoxazole-3-carbohydrazide (5h)

Pale yellow crystalline (65.2%); $R_f = 0.50$; m.p.: 215–216 °C; ^{1}H NMR (300 MHz, DMSO-d6): $\delta = 2.33$ (s, 3H, CH_3), 3.83 (s, 1H, OCH_3), 6.78 (dd, 1H, Ar-H, $J = 4.8$ Hz, 4.8 Hz), 7.09–7.40 (m, 1H, Ar-H), 7.48 (s, 1H, isoxazole CH), 7.55–7.58 (m, 4H, Ar-H), 7.92–7.97 (m, 2H, Ar-H), 9.53 (s, 1H, CONH), 11.02 (s, 1H, OH). ^{13}C NMR (75 MHz, DMSO-d6): $\delta = 15.07$ (CH_3), 56.11 (OCH_3), 100.65 (isoxazole CH), 110.57, 115.53, 121.04, 126.28 (2C), 126.73, 129.17, 129.85 (2C), 131.40, 147.92, 149.35, 155.70, 159.03, 159.64, 170.77. IR (KBr): 3329.28 (OH), 3288.77 (NH), 3051.52 (Ar C −H), 1682.00 (NH-C=O), 1571.09 (C=N), 1512.26 (C=C, isoxazole), 1448.60 cm^{-1} (Ar C=C); ESI-MS (*m/z*): 352.38 (M + 1); Anal. for $C_{19}H_{17}N_3O_4$: calcd: C 64.95, H 4.88, N 11.96, found: C 65.14, H 5.03, N 11.77.

N′-(1-(3-hydroxyphenyl)ethylidene)-5-phenylisoxazole-3-carbohydrazide (5i)

Buff colored crystalline (90.5%); $R_f = 0.52$; m.p.: 225–226 °C; ^{1}H NMR (400 MHz, DMSO-d6): $\delta = 2.35$ (s, 3H, CH_3), 6.85–6.88 (m, 1H, Ar-H), 7.23–7.28 (m, 2H, Ar-H), 7.36 (s, 1H, isoxazole CH), 7.51–7.56 (m, 1H, Ar-H), 7.58–7.60 (m, 3H, Ar-H), 7.96–7.98 (m, 2H, Ar-H), 9.61 (s, 1H, CONH), 11.06 (s, 1H, OH). ^{13}C NMR (100 MHz, DMSO-d6): $\delta = 14.66$ (CH_3), 100.22 (isoxazole CH), 113.01, 117.09, 117.67, 125.78 (2C), 126.22, 129.34 (2C), 129.40 (2C), 130.91, 138.89, 155.54, 157.31, 159.05, 170.33; IR (KBr): 3336.99 (OH), 3280.09 (NH), 3055.38 (Ar C-H), 1669.46 (NH-C=O), 1603.88 (C=N), 1507.43 (C=C, isoxazole), 1444.75 cm^{-1} (Ar C=C); ESI-MS (*m/z*): 322.39 (M + 1); Anal. for $C_{18}H_{15}N_3O_3$: calcd: C 67.28, H 4.71, N 13.08, found: C 67.54, H 4.82, N 13.41.

N′-(1-(3-nitrophenyl)ethylidene)-5-phenylisoxazole-3-carbohydrazide (5j)

White shiny crystalline (73.9%); $R_f = 0.46$; m.p.: 222–223 °C; ^{1}H NMR (400 MHz, DMSO-d6): $\delta = 2.47$ (s, 3H, CH_3), 7.53–7.61 (m, 4H, Ar-H), 7.74–7.78 (t, 1H, Ar-H, $J =$ 8.0 Hz), 7.96–7.99 (m, 2H, Ar-H), 8.28–8.31 (m, 2H, Ar-H), 8.65 (s, 1H, isoxazole CH), 11.28 (s, 1H, CONH). ^{13}C NMR (100 MHz, DMSO-d6): $\delta = 14.65$ (CH_3), 100.27 (isoxazole CH), 120.83, 124.21, 125.79 (2C), 126.17, 129.35 (2C), 130.13, 130.94, 132.94, 139.23, 147.96, 154.68, 155.92, 158.86, 170.41. IR (KBr): 3336.03 (NH), 3064.06 (Ar C-H), 1696.47 (NH-C=O), 1570.12 (C=N), 1517.08 (C=C, isoxazole), 1496.83 (Ar N-O), 1448.60 (Ar C=C), 1350.23 cm^{-1} (Ar N-O). ESI-MS (*m/z*): 351.34 (M + 1); Anal. for $C_{18}H_{14}N_4O_4$: calcd: C 61.71, H 4.03, N 15.99, found: C 61.95, H 4.45, N 16.15.

Ethical approval

Animal studies were performed after approval from the Institutional Animal Ethical Committee of the GLA University, Mathura (Approval no. GLAIPR/CPCSEA/IAEC/2016/ItemII/6; 2018/ItemII/3). Wistar rats (220–250 g) and male mice (20–25 g) of at least eight weeks of age were used for the study.

In vitro MAO inhibitory activity

Materials

p-Tyramine for the MAO-A and MAO-B assay, reference inhibitors clorgyline (MAO-A), pargyline (MAO-B), Amplex Red reagent and horseradish peroxidase were procured from Sigma-Aldrich.

Isolation of mitochondria from rat brain

For isolation of MAO enzyme containing mitochondrial fractions from rat brain, the procedure of Iglesias-González et al. (Iglesias-González et al. 2013) was followed. Rats were fasted overnight with free access to water and sacrificed by cervical dislocation and decapitated. The brain was then rapidly removed and kept in an ice-cold isolation buffer. The ice-cold conditions were maintained throughout the isolation procedure.

Forebrain was carefully removed and the remaining tissues were chopped and homogenized using isolation buffer (1/10, w/v) supplemented with 3 mM EDTA. The homogenate was suspended in 10 mL isolation buffer and centrifuged at $600 \times g$ for 10 min. The supernatant was separated and reserved in a chilled recipient, and the pellet was centrifuged again after resuspending in 10 mL of buffer. The supernatants were pooled and further centrifuged at $12{,}000 \times g$ for 10 min. The mitochondrial pellets so obtained were washed three times with isolation buffer supplemented with EDTA and stored at −20 °C until the assay.

Enzyme inhibition assay

The mitochondrial pellet so obtained above was suspended in a suitable amount of reaction buffer (0.1 M Phosphate buffer, pH 7.2) and divided into two parts. One part was incubated with clorgyline (1 μM, a selective inhibitor of MAO-A) and another one with pargyline (1 μM, a selective inhibitor of MAO-B) for 30 min to get MAO-B and MAO-A

enzyme fractions, respectively (Chimenti et al. 2007). Ten µL of each enzyme fractions were pre-incubated with different concentrations (0.5 nM, 5 nM, 50 nM, 500 nM, 5 µM, and 50 µM) of test compounds (**5a-j**) for 15 min in a black flat-bottomed 96-well micro test plate followed by addition of Amplex Red reagent (200 µM), horseradish peroxidase (1 U/mL) and *p*-tyramine (500 µM) to start the reaction. The production of fluorescent resorufin in the reaction mixture (total 100 µL) was measured at 37 °C in a microplate fluorescence reader (Biotek, Synergy H1, Winooski, VT, USA) over a 15 min period (excitation 540 nm, emission 590 nm). All the assays were performed in triplicate.

Control experiments were carried out simultaneously using vehicles in place of the test drugs, and the background activity was determined without the mitochondrial fraction replaced by sodium phosphate buffer solution. The background activity was found to be negligible. The possible capacity of the test compounds and reference inhibitors to modify the fluorescence (by directly interacting with Amplex Red reagent) were determined by adding these drugs to solutions containing only the Amplex Red reagent in sodium phosphate buffer.

Statistical analysis

IC_{50} values are calculated using the non-linear curve-fitting program of the GraphPad Prism 6.01 (San Diego, CA, USA) from the sigmoidal plots of MAO catalytic rate *versus* the logarithm of the inhibitor concentration, and results are expressed in mean ± SEM ($n = 3$).

Reversibility study

To determine the reversibility of most active MAO-B inhibitors, i.e. **5d** and **5g**, the dilution method was used (Copeland 2005). A 100-fold concentration required for the activity assay of the enzyme was incubated with the inhibitor (10-fold concentration of its IC_{50} value). After 30 min, the mixture was diluted 100-fold with reaction buffer containing the substrate, Amplex Red reagent and horseradish peroxidase. The reaction was monitored for 15 min. Reversible inhibitors show linear progress with a slope equal to ~91% of the slope of the control sample, whereas irreversible inhibition reaches only ~9% of this slope. Control tests were carried out by pre-incubating and diluting the enzyme in the absence of inhibitor.

Kinetic analysis of inhibition

The Michaelis-Menten kinetic experiments were performed to determine the mode of inhibition of most potent compounds **5d** and **5g**. Briefly, the catalytic rate of MAO-B was estimated taking different concentrations of the substrate (250, 500, 750, 1000 µM) in the absence and presence of three different concentrations (½ × IC_{50}, 1 × IC_{50} and 1½ × IC_{50}) of compounds **5d** and **5g**, i.e., 0.0025, 0.005 and 0.0075 µM; and the Lineweaver-Burk plots were generated. The *Ki* values were estimated from a plot of the slopes of the Lineweaver-Burk plots *versus* inhibitor concentration (x-axis intercept equals *–Ki*). The protein content of the mitochondrial homogenate was determined using the Bradford assay method (Bradford 1976) in which bovine serum albumin was used as a standard.

Molecular docking studies

In an attempt to acquire the understanding of possible binding modes of the synthesized compounds with the human MAO-B active site, molecular docking study was performed using Autodock 4.2 program suite (Morris et al. 2009). The X-ray crystal structure of human MAO-B co-crystallized with a coumarin analog (PDB ID: 2V60, resolution: 2 Å) was retrieved from RCSB Protein Data Bank (Binda et al. 2007). The protein was prepared for molecular docking simulations by removing chain-B and bound ligand from the dimeric complex structure of MAO-B. Further it was subjected to the addition of hydrogen atoms and Gasteiger partial charges followed by merging non-polar hydrogens. Nine water molecules that have been found important for mediating the interactions of inhibitors were conserved and thus included in the docking process (Distinto et al. 2012). All the residues of the MAO-B binding site were considered as rigid while all the single bonds of the ligands were considered rotatable for the docking simulation. The receptor grid was generated with a grid box size of 50 × 50 × 50, the spacing of 0.503 Å and centered on the ligand. Before docking the test compounds, the docking protocol was validated by running docking simulations with the bound ligand. The RMSD below 0.2 Å indicates good predictability power of docking protocol. The Lamarckian genetic algorithm searches were used to perform 10 runs, and the default docking protocol was used with an initial population of 50 randomly placed individuals, a maximum number of 2.5×10^6 energy evaluations and a maximum number of 2.7×10^4 generations. A top scoring molecule with the most favorable free energy of binding from the cluster on the basis of lowest binding energy was considered for the further analysis. 2D and 3D interaction plots between protein and ligand were generated using Biovia Discovery Studio Visualizer 2017 R2.

Acute toxicity study

The acute toxicity of compounds **5d** and **5g** was performed at dose levels of 175, 550 and 2000 mg Kg^{-1} body

weight orally in mice, as per OECD-425 guidelines (OECD 2008) and were observed for mortality after 24 h for short-term toxicity and for 14 days to record the long-term toxicity.

Neurotoxicity screening

To evaluate the possible neurotoxicity of the compounds **5d** and **5g**, rotarod apparatus was employed (Krall et al. 1978). For which, the albino mice (20–25 g) were used as experimental animals and allowed food and water ad libitum. Before screening the mice were trained to stay on a rotating rod (3.2 cm diameter) rotating at six revolutions per minute for the 60 s. Trained animals were grouped containing six animals in each. The compounds under study were administered by *p.o.* route suspended in 0.2% carboxymethylcellulose (CMC) at a dose of 200 mg Kg^{-1}. The neurotoxicity was judged on the basis of the number of animals falling within the stipulated time of the 60 s.

Motor behavioral test

The in vivo efficacy of compounds **5d** and **5g** to inhibit MAO-B was evaluated in the MPTP-induced mouse model of PD (Jackson-Lewis and Przedborski 2007). The detailed experimental schedule is depicted in Fig. 4. Animals were randomly divided into nine groups. The groups were control, MPTP, Safinamide (standard), 5d-50, 5d-100, 5d-200, 5g-50, 5g-100 and 5g-200. The mice ($n = 6$) were orally administered standard Safinamide (30 mg Kg^{-1}), different doses of compounds **5d** or **5g** (50, 100, 200 mg Kg^{-1}) suspended in 0.2% CMC every 24 h for three consecutive days (day 0, 1 and 2). On day 1, MPTP dissolved in saline (2 mg mL^{-1}) was administered intraperitoneally (20 mg Kg^{-1} for one injection) four times at 2 h interval. On the seventh day of MPTP administration, the mice were subjected to behavioral tasks, i.e., footprint and horizontal wire tests with a lag of 30 min between two tasks. These tests are used to evaluate PD-like motor dysfunctions in mice (Kasahara et al. 2017).

In the footprint test, the experimental mice were trained to walk straight on a 60 cm long runway with a white paper toward a dark goal-box at the end. On the test day, the fore- and hind-paws of mice were dyed with different colors and made to walk on the runway to the goal to analyze abnormal gait. The footprint patterns obtained on the paper were then manually analyzed for stride length and base width for both fore- and hind-paws.

The horizontal wire test measures the motor coordination and muscle relaxation in experimental animals. In this test, mice are lifted by the tail and allowed to grasp a wire (30 cm long) stretched 30 cm horizontally above the ground platform with their fore-paws and then released. The grip strength was scored according to the following scale: 0—if the mice fall off the wire; 1—hangs onto wire by two fore-paws; 2—attempts to climb on the wire while holding it with fore-paws; 3—grasps the wire with one or both hind paws too; 4—wraps the tail around the wire while holding it with all the paws; 5—reaches to the one end of the wire and escapes from the apparatus (Geed et al. 2014). The mice were trained for this task for 2–3 times before MPTP administration.

Acknowledgements The authors are thankful to the authorities of GLA University, Mathura, India for their praiseworthy inspiration and providing the facilities for this project.

Compliance with ethical standards

Conflict of interest The authors declare that they have no conflict of interest.

References

Agrawal N, Mishra P (2018) The synthetic and therapeutic expedition of isoxazole and its analogs. Med Chem Res 27:1309–1344. https://doi.org/10.1007/s00044-018-2152-6

Bach AWJ, Lan NC, Johnson DL et al. (1988) cDNA cloning of human liver monoamine oxidase A and B: Molecular basis of differences in enzymatic properties. Proc Natl Acad Sci USA 85:4934–4938

Binda C, Hubálek F, Li M et al. (2004) Crystal structure of human monoamine oxidase B, a drug target enzyme monotopically inserted into the mitochondrial outer membrane. FEBS Lett 564:225–228. https://doi.org/10.1016/S0014-5793(04)00209-1

Binda C, Wang J, Pisani L et al. (2007) Structures of human monoamine oxidase B complexes with selective noncovalent inhibitors: safinamide and coumarin analogs. J Med Chem 50:5848–5852. https://doi.org/10.1021/jm070677y

Bradford MM (1976) A rapid and sensitive method for the quantitation of microgram quantities of protein utilizing the principle of protein-dye binding. Anal Biochem 72:248–254. https://doi.org/10.1016/0003-2697(76)90527-3

Chimenti F, Maccioni E, Secci D et al. (2007) Selective inhibitory activity against MAO and molecular modeling studies of 2-thiazolylhydrazone derivatives. J Med Chem 50:707–712. https://doi.org/10.1021/jm060869d

Chimenti F, Secci D, Bolasco A et al. (2010a) Synthesis, stereochemical separation, and biological evaluation of selective inhibitors of human MAO-B: 1-(4-Arylthiazol-2-yl)-2-(3-methylcyclohexylidene)hydrazines. J Med Chem 53:6516–6520. https://doi.org/10.1021/jm100120s

Chimenti F, Secci D, Bolasco A et al. (2010b) Synthesis and selective inhibition of human monoamine oxidases of a large scaffold of (4,5-substituted-thiazol-2-yl)hydrazones. Medchemcomm 1:61–72. https://doi.org/10.1039/c0md00014k

Copeland RA (2005) Evaluation of enzyme inhibitors in drug discovery. A guide for medicinal chemists and pharmacologists. John Wiley & Sons, Inc., New Jersey

Distinto S, Meleddu R, Yanez M et al. (2016) Drug design, synthesis, in vitro and in silico evaluation of selective monoaminoxidase B inhibitors based on 3-acetyl-2-dichlorophenyl-5-aryl-2,3-dihydro-

1,3,4-oxadiazole chemical scaffold. Eur J Med Chem 108:542–552. https://doi.org/10.1016/j.ejmech.2015.12.026

Distinto S, Yáñez M, Alcaro S et al. (2012) Synthesis and biological assessment of novel 2-thiazolylhydrazones and computational analysis of their recognition by monoamine oxidase B. Eur J Med Chem 48:284–295. https://doi.org/10.1016/j.ejmech.2011.12.027

Edmondson DE, Binda C, Mattevi A (2007) Structural insights into the mechanism of amine oxidation by monoamine oxidases A and B. Arch Biochem Biophys 464:269–276. https://doi.org/10.1016/j.abb.2007.05.006

Evranos-Aksöz B, Yabanoğlu-Çiftçi S, Uçar G et al. (2014) Synthesis of some novel hydrazone and 2-pyrazoline derivatives: Monoamine oxidase inhibitory activities and docking studies. Bioorganic Med Chem Lett 24:3278–3284. https://doi.org/10.1016/j.bmcl.2014.06.015

Fabbri M, Rosa MM, Ferreira JJ (2016) Clinical pharmacology review of opicapone for the treatment of Parkinson's disease. Neurodegener Dis Manag 6:349–362. https://doi.org/10.2217/nmt-2016-0022

Geed M, Garabadu D, Ahmad A, Krishnamurthy S (2014) Silibinin pretreatment attenuates biochemical and behavioral changes induced by intrastriatal MPP + injection in rats. Pharmacol Biochem Behav 117:92–103. https://doi.org/10.1016/j.pbb.2013.12.008

Geha RM, Rebrin I, Chen K, Shih JC (2001) Substrate and inhibitor specificities for human monoamine oxidase a and b are influenced by a single amino acid. J Biol Chem 276:9877–9882. https://doi.org/10.1074/jbc.M006972200

Grimsby J, Lan NC, Neve R et al. (1990) Tissue distribution of human monoamine oxidase A and B mRNA. J Neurochem 55:1166–1169. https://doi.org/10.1111/j.1471-4159.1990.tb03121.x

Hauptmann N, Grimsby J, Shih JC, Cadenas E (1996) The metabolism of tyramine by monoamine oxidase A/B causes oxidative damage to mitochondrial DNA. Arch Biochem Biophys 335:295–304. https://doi.org/10.1006/abbi.1996.0510

Huggins DJ, Sherman W, Tidor B (2012) Rational approaches to improving selectivity in drug design. J Med Chem 55:1424–1444. https://doi.org/10.1021/jm2010332

Iglesias-González J, Sánchez-Iglesias S, Beiras-Iglesias A et al. (2013) A simple method for isolating rat brain mitochondria with high metabolic activity: Effects of EDTA and EGTA. J Neurosci Methods 213:39–42. https://doi.org/10.1016/j.jneumeth.2012.12.005

Jackson-Lewis V, Przedborski S (2007) Protocol for the MPTP mouse model of Parkinson's disease. Nat Protoc 2:141–151. https://doi.org/10.1038/nprot.2006.342

Jha SK, Jha NK, Kumar D et al. (2017) Linking mitochondrial dysfunction, metabolic syndrome and stress signaling in neurodegeneration. Biochim Biophys Acta Mol Basis Dis 1863:1132–1146. https://doi.org/10.1016/j.bbadis.2016.06.015

Kasahara J, Choudhury ME, Nishikawa N et al. (2017) Neurotoxin 1-methyl-4-phenyl-1,2,3,6-tetrahydropyridine (MPTP)-induced animal models of parkinson's disease. In: Conn PM (ed) Animal models for the study of human disease, 2nd edn. Elsevier, London, pp 1087–1108

Krall RL, Penry JK, White BG et al. (1978) Antiepileptic drug development: II. Anticonvulsant drug screening. Epilepsia 19:409–428

Kumar B, Sheetal S, Mantha AK, Kumar V (2016) Recent developments on the structure–activity relationship studies of MAO inhibitors and their role in different neurological disorders. RSC Adv 6:42660–42683. https://doi.org/10.1039/C6RA00302H

Lipinski CA, Lombardo F, Dominy BW, Feeney PJ (2012) Experimental and computational approaches to estimate solubility and permeability in drug discovery and development settings. Adv Drug Deliv Rev 64:4–17. https://doi.org/10.1016/j.addr.2012.09.019

Ma J, Yoshimura M, Yamashita E et al. (2004) Structure of rat monoamine oxidase A and its specific recognitions for substrates and inhibitors. J Mol Biol 338:103–114. https://doi.org/10.1016/j.jmb.2004.02.032

Maccioni E, Alcaro S, Cirilli R et al. (2011) 3-Acetyl-2,5-diaryl-2,3-dihydro-1,3,4-oxadiazoles: a new scaffold for the selective inhibition of monoamine oxidase B. J Med Chem 54:6394–6398. https://doi.org/10.1021/jm2002876

Meleddu R, Distinto S, Cirilli R et al. (2017) Through scaffold modification to 3,5-diaryl-4,5-dihydroisoxazoles: new potent and selective inhibitors of monoamine oxidase B. J Enzyme Inhib Med Chem 32:264–270. https://doi.org/10.1080/14756366.2016.1247061

Morris GM, Huey R, Lindstrom W et al. (2009) AutoDock4 and AutoDockTools4: automated docking with selective receptor flexibility. J Comput Chem 30:2785–2791. https://doi.org/10.1002/jcc.21256

Nam M, Park M, Park H et al. (2017) Indole-substituted benzothiazoles and benzoxazoles as selective and reversible MAO-B inhibitors for treatment of parkinson's disease. ACS Chem Neurosci 8:1519–1529. https://doi.org/10.1021/acschemneuro.7b00050

Nicotra A, Pierucci F, Parvez H, Senatori O (2004) Monoamine oxidase expression during development and aging. Neurotoxicology 25:155–165. https://doi.org/10.1016/S0161-813X(03)00095-0

OECD (2008) Test No. 425: acute oral toxicity: up-and-down procedure. OECD guidelines for the testing of chemicals, section 4. OECD publishing, Paris

Salgın-Gökşen U, Gökhan-Kelekçi N, Yabanoglu-Çiftci S et al. (2013) Synthesis, molecular modeling, and in vitro screening of monoamine oxidase inhibitory activities of some novel hydrazone derivatives. J Neural Transm 120:883–891. https://doi.org/10.1007/s00702-013-0968-2

Shih JC, Chen K, Ridd MJ (1999) Monoamine oxidase: from genes to behavior. Annu Rev Neurosci 22:197–217. https://doi.org/10.1146/annurev.neuro.22.1.197

Taha M, Ismail NH, Javaid K et al. (2015) Evaluation of 2-indolcarbohydrazones as potent α-glucosidase inhibitors, in silico studies and DFT based stereochemical predictions. Bioorg Chem 63:24–35. https://doi.org/10.1016/j.bioorg.2015.09.001

Tipton KF (1986) Enzymology of monoamine oxidase. Cell Biochem Funct 4:79–87. https://doi.org/10.1002/cbf.290040202

Veeraswamy B, Kurumurthy C, Santhosh Kumar G et al. (2012) Synthesis of novel 5-substituted isoxazole-3-carboxamide derivatives and cytotoxicity studies on lung cancer cell line. Indian J Chem Sect B Org Med Chem 51:1369–1375

Waterhouse RN (2003) Determination of lipophilicity and its use as a predictor of blood-brain barrier penetration of molecular imaging agents. Mol Imaging Biol 5:376–389. https://doi.org/10.1016/j.mibio.2003.09.014

Weyler W, Hsu YPP, Breakafield XO (1990) Biochemistry and genetics of monoamine oxidase. Pharmacol Ther 47:391–417. https://doi.org/10.1016/0163-7258(90)90064-9

Yamada M, Yasuhara H (2004) Clinical pharmacology of MAO inhibitors: safety and future. Neurotoxicology 25:215–221

Youdim MBH, Edmondson D, Tipton KF (2006) The therapeutic potential of monoamine oxidase inhibitors. Nat Rev Neurosci 7:295–309. https://doi.org/10.1038/nrn1883